Title: A diencephalic pathway for movement initiation and rescue of Parkinsonian symptoms

Authors/Affiliations:

Glenn D.R. Watson[1], Ryan N. Hughes[1*], Elijah A. Petter[1*], Henry H. Yin[1,2,†]

1. Department of Psychology and Neuroscience, Duke University, Durham, NC, 27708, USA., 2. Department of Neurobiology, Duke University School of Medicine, Durham, NC, 27708, USA.

†**Corresponding author**. E-mail: hy43@duke.edu

Abstract

The parafascicular nucleus (Pf) of the thalamus sends major projections to the basal ganglia, a group of subcortical nuclei involved in action initiation and selection. Here, we used optogenetics, 3D motion capture, in vivo electrophysiology, and viral-based neuroanatomical tracing to examine the contribution of the Pf to volitional movements in mice. We discovered that Pf neurons are highly correlated with movement velocity. Stimulation of glutamatergic (Vglut2+) neurons in the Pf generates turning and orienting movements. This effect was not due to Pf projections to the striatum, but to its projections to the subthalamic nucleus (STN), a major target of deep brain stimulation (DBS) for Parkinson's disease (PD) patients. Moreover, selective excitation of either Pf Vglut2+ terminals in the STN or Pf cell bodies that send glutamatergic projections to the STN can restore natural movements in a bilateral mouse model of PD with complete akinesia. Our results reveal a novel thalamo-subthalamic pathway regulating movement initiation, and demonstrate a circuit mechanism that could explain the clinical efficacy of DBS for relief of Parkinson's disease motor symptoms.

One Sentence Summary

Excitation of the Pf-STN pathway generates movements and rescues akinesia in Parkinsonian mice.

The parafascicular nucleus (Pf) is a midline thalamic region strongly connected with the basal ganglia (BG), a set of subcortical nuclei critical for action initiation (*1*). Recent studies have attempted to elucidate the functional significance of Pf interactions with the BG, with emphasis on the thalamostriatal projections (*2, 3*). Studies suggest that the Pf can modulate striatal activity, and pharmacological manipulations produce deficits in arousal, learning, and behavioral flexibility (*4, 5*). In humans, deep brain stimulation (DBS) in the centromedian/parafascicular complex is an emerging therapeutic target for the treatment of Parkinson's disease (PD). DBS of both the Pf and the subthalamic nucleus (STN) ameliorate key motor symptoms of PD (*6*). Yet little is known about how the Pf contributes to movement or the mechanisms underlying the efficacy of DBS in this region for the treatment of PD.

To understand the contribution of Pf to movement, we optogenetically stimulated Pf neurons while monitoring movement kinematics with 3D motion capture (Fig. 1, A and B). Unilateral photo-excitation of Pf neurons produces ipsiversive turning (10 mW, 5 ms pulses, neurons infected with an adeno-associated virus (AAV) under a ubiquitous neuronal promoter, AAV5.Syn.Chronos.GFP.WPRE.bGH, n = 7, Fig. S1). To limit the stimulation to gluamatergic projection neurons (Vglut2+), we injected a virus with Cre-dependent channelrhodopsin (ChR2) in Vglut2-Cre mice transgenic mice (n = 6, Fig. 1C-F; Movie S1). Increasing the stimulation frequency also increases the speed of turning (Fig. 1F, left; Fig. S1B, left). Furthermore, a single laser pulse produces a relatively fixed amount of turning regardless of the frequency of stimulation (Fig. 1F, right; Fig. S1B, right). Bilateral excitation, however, slows movement throughout the stimulation period (Fig. S1C).

On the other hand, inhibition with halorhodopsin had no significant effects on movement (Fig. 1, C-E; Vglut2::eNpHR3.0^{Pf}, n = 6; Vglut2::eYFP^{Pf} control mice, n = 6). Because optogenetic inhibition might not be sufficient to shut down Pf activity in a normally behaving animal(*7*), we injected muscimol, a potent $GABA_A$ agonist, to inactivate the Pf (Fig. 1G; n = 8). Unilateral muscimol injections produced contraversive turning in a dose-dependent manner (Fig. 1G, right; Movie S2). Thus Pf excitation and inhibition appear to have opposite effects on turning behavior.

To understand the relationship between Pf activity and movement, we wirelessly recorded in vivo single-unit activity in the Pf and tracked movements with 3D motion capture (*8,*

9). This task allows us to record neural activity during continuous, self-initiated orienting and turning behavior while mice tracked a moving sucrose reward (Fig. 2A). We found that a subset of neurons in the Pf encode velocity, primarily in the ipsiversive direction (27%) relative to the recording hemisphere (Fig. 2B, top). These neurons show a highly linear relationship with ipsiversive velocity (Fig. 2, C and D; n = 21). On the other hand, far fewer Pf neurons were found to encode contraversive velocity (Fig. 2B, bottom; Fig. S2; 5%). This is the first report of such a robust and continuous relationship with ipsiversive turning velocity anywhere in the brain.

Our single unit recording data are in accord with our open-field excitation results, suggesting that the Pf contains neurons could drive ipsiversive turning. Two major targets of the Pf are the striatum and STN, which are both involved in basal ganglia circuits for action initiation (*10, 11*). We confirmed Pf projections to both regions in mice through viral-based neuroanatomical tracing by injecting a high-titer of canine adenovirus type 2 with Cre recombinase (CAV2-Cre) into Ai-14 reporter mice (Fig. 3A). A high titer of CAV2-Cre allows for the visualization of both Pf afferent and efferent connectivity (Fig. S3). We show that, in mice, the Pf also contains two distinct neuronal populations that send distinct projections to the striatum and STN (Fig. 3B, n = 3), in agreement with previous work in rats(*12*).

To elucidate their functional contributions, we separately excited thalamostriatal and thalamo-subthalamic glutamatergic terminals. We injected a Cre-dependent virus containing ChR2 into the Pf of Vglut2-Cre mice (Fig. 3C; Vglut2::ChR2 $^{\text{Pf-STN}}$, n = 8; Vglut2::ChR2 $^{\text{Pf-Striatum}}$, n = 7), but not Pf thalamostriatal neurons produce ipsiversive turning (Fig. 3, D-F; Movie S3). This turning effect is very similar to that observed during Pf cell-body excitation (Fig. 1, C and D).

We replicated our Pf cell-body stimulation results using a virus with retrograde access to projection neurons(*13*). We injected AAV(retro2).hSyn.EF1α.Cre.WPRE into the downstream region of interest and rAAV5.EF1α.DIO.hChR2(H134R).eYFP into the Pf of wild type mice (Fig. S4; Wildtype.Retro::ChR2$^{\text{Pf-Striatum}}$, n = 7; Wildtype.Retro::ChR2, n =7). This strategy allows us to excite only the Pf neurons that project to the STN. Unlike the movements evoked from pathway non-specific excitation, excitation of the Pf-STN pathway increases forward velocity and does not slow movement during bilateral stimulation (Fig. S4B).

The difference between our Pf-STN and Pf-striatum effects cannot simply be explained

by differences in penetrance or size of the target region, as the thalamostriatal projections are more massive and target a larger area. If anything, this would predict a larger effect of thalamostriatal activation, but the opposite was observed. More importantly, it is well established that striatal activation produces contraversive rather than ipsiversive movements(*14*). Our observation of ipsiversive turning therefore supports an extra-striatal route by which Pf influences turning.

To further reveal the circuitry responsible for ipsiversive turning, we sought to determine the downstream targets of STN neurons that receive Pf projections. To visualize Pf-defined STN projections, we first injected AAV1.hSyn.tdTomato.Cre into the Pf (Fig. 3G). This virus displays anterograde transsynaptic spread (*15*). We then injected a cre-dependent virus (AAV5-DIO-eYFP) into the STN. In other words, only STN neurons that are postsynaptic targets of the Pf will express eYFP. We found that Pf-defined STN efferents terminated in various BG output nuclei, including the substantia nigra pars reticulata (SNr), the external globus pallidus (GPe), the entopeduncular nucleus (EP, the rodent homologue of the internal globus pallidus), as well as other key subcortical regions for motor control (Fig. 3, H and I; n = 3). This finding shows that, independently of the striatum, the major BG input nucleus, the Pf can influence BG output via the STN. This is in agreement with the previous observation that activation of BG output nuclei like the SNr (*16*).

Our results suggest a novel circuit mechanism for DBS. At least some of the therapeutic effects of conventional STN-DBS may be due to stimulation of the Pf-STN pathway. To test this hypothesis, we used a common rodent PD model in which dopamine neurons from the substantia nigra pars compacta (SNc) are depleted by injecting 6-hydroxydopamine (6-OHDA) into the medial forebrain bundle (mfb) bilaterally. Bilateral dopamine depletion produced nearly complete akinesia in mice. To test whether selective excitation of Pf-STN projections can rescue akinesia, we stimulated Vglut2+ Pf-STN terminals (Fig. 4A; Vglut2.PD::ChR2$^{Pf\text{-}STN}$, n = 5), and quantified the movements of bilateral-PD mice (Fig. 4, B and C; Movie S4). Photo-excitation resulted in a dramatic increase in movement and the average distance traveled (Fig. 4, C and D). A similar improvement was found during cell-body excitation (Fig. S5; Movie S5; Wild-type.Retro.PD::ChR2$^{Pf\text{-}STN}$, n = 5), but not inhibition (Vglut2.Retro.PD::eNpHR3.0$^{Pf\text{-}STN}$, n = 3; Movie S6) of Pf-STN neurons.

Spontaneous behaviors can be highly diverse. While traditional behavioral measures

only focus on some aspect of movement (e.g. distance travelled or kinematics), they do not provide a comprehensive view of different types of behaviors affected by a neural manipulation. To quantify natural behavioral states, we applied an Autoregressive Hidden Markov model (AR-HMM) on the video recordings during our rescue experiments (*17*). The AR-HMM revealed distinct behavioral states as a result of stimulation (Fig. 4E; Movie S7). If we compare the baseline akinetic condition to stimulation conditions, stimulation restored multiple natural behaviors such as rearing, turning, ambulation, and exploration, and reduced immobility. As Fig. 4F shows, stimulation increases the transition probabilities among different kinetic states, but reduces transition from kinetic to akinetic states.

Our findings demonstrate that the Pf could be a part of a circuit for orienting and steering in mice. Given the strong afferents from neuromodulatory and multimodal sensory brain regions (Fig. 3I; Fig. S6), the Pf is in a position to combine somatosensory and proprioceptive information to form representations of movement kinematics, especially velocity. In support of this conclusion, we identified a subset of Pf neurons that are highly correlated with turning velocity, in agreement with our optogenetic excitation results (Fig. 1, C and F). Moreover, we identified downstream brain regions that could mediate the movement effects observed by Pf-STN excitation with transsynaptic tracing (Fig. 3, G-I). We thus uncovered a key node in the neural network for left-right steering, with the Pf from each hemisphere responsible for ipsiversive movements.

Bilateral Pf Vglut2+ excitation resulted in slowed movement likely due to simultaneous activation of antagonistic units (e.g., leftward and rightward) from the two hemispheres (Fig. S1C). However, we did not observe this phenomenon during bilateral STN excitation (Fig. S4B). It is possible that recruitment of both Pf thalamostriatal and thalamo-subthalamic neurons produces a conflict at longer stimulation durations and does not mimic the natural activation pattern of this circuit.

With conventional DBS, it is impossible to determine whether the therapeutic effect is due to activating local neural populations, presynaptic axon terminals, or fibers of passage. Nor is it entirely clear whether DBS excites or inhibits local neural elements. As CM/Pf- and STN-DBS both ameliorate key motor symptoms of PD, it is possible that the effect of STN-DBS could be due to exciting Pf input to the STN. Our study supports this hypothesis by demonstrating rescue of akinesia in bilateral-PD mice using selective targeting of the Pf-STN

pathway (Fig. 4; Fig. S5).

Previous work showed that optogenetic stimulation of local STN neurons does not rescue akinesia, but that inputs from the motor cortex were more important (*18*). These results suggest the possibility that conventional DBS produces antidromic activation of neurons presynaptic to the STN. Here we show that Pf is a key region upstream of the STN that is responsible for DBS rescue of PD symptoms. By exciting thalamic projections to the STN, we were able to restore natural movements in bilateral-PD mouse models, supporting the possibility that the therapeutic effects of STN-DBS are derived from activating Pf glutamatergic afferents to the STN. A recent study demonstrates increased locomotion in dopamine depleted mice by optogenetically exciting parvalbumin-positive neurons in the GPe(*19*). Interestingly, these GPe neurons also project to the Pf (*20*), suggesting a potential circuit that can be recruited to generate movement in Parkinsonian mice.

We were able to restore and increase the transition probability of numerous natural behavioral states that are difficult to quantify with conventional measures. For instance, Pf-STN excitation alleviates numerous axial symptoms, such as gait immobility, and promotes natural postural rearing (Fig. 4, D and E; Fig. S5). Such symptoms that are not satisfactorily treated with conventional DBS approaches and are often resistant to medication (*6, 21, 22*). It is possible that stimulating CM/Pf input to the STN in PD patients could abolish pathological STN activity, thus restoring movement (*23, 24*). Research is needed to elucidate the synaptic and circuit-wide consequences of thalamo-subthalamic excitation in PD. Additional research is needed to elucidate the synaptic and circuit-wide consequences of thalamo-subthalamic excitation in PD.

One surprising result from our study is that the massive Pf-striatum projections are not critical for movement initiation. It is possible that the Pf afferents to the striatum could contribute to higher functions, such as decision making and behavioral flexibility, but do not generate movement per se (*25*). Collectively, our results suggest that Pf-STN projections represent a diencephalic analogue of the 'hyperdirect' pathway from the cortex to the STN, allowing the Pf to have direct access to BG output nuclei and other regions critical for movement initiation (*26*). Pf-STN projections may therefore serve as a rapid orienting mechanism to shift the body towards a salient stimulus, while Pf thalamostriatal projections can influence the selection of the next

behavioral program.

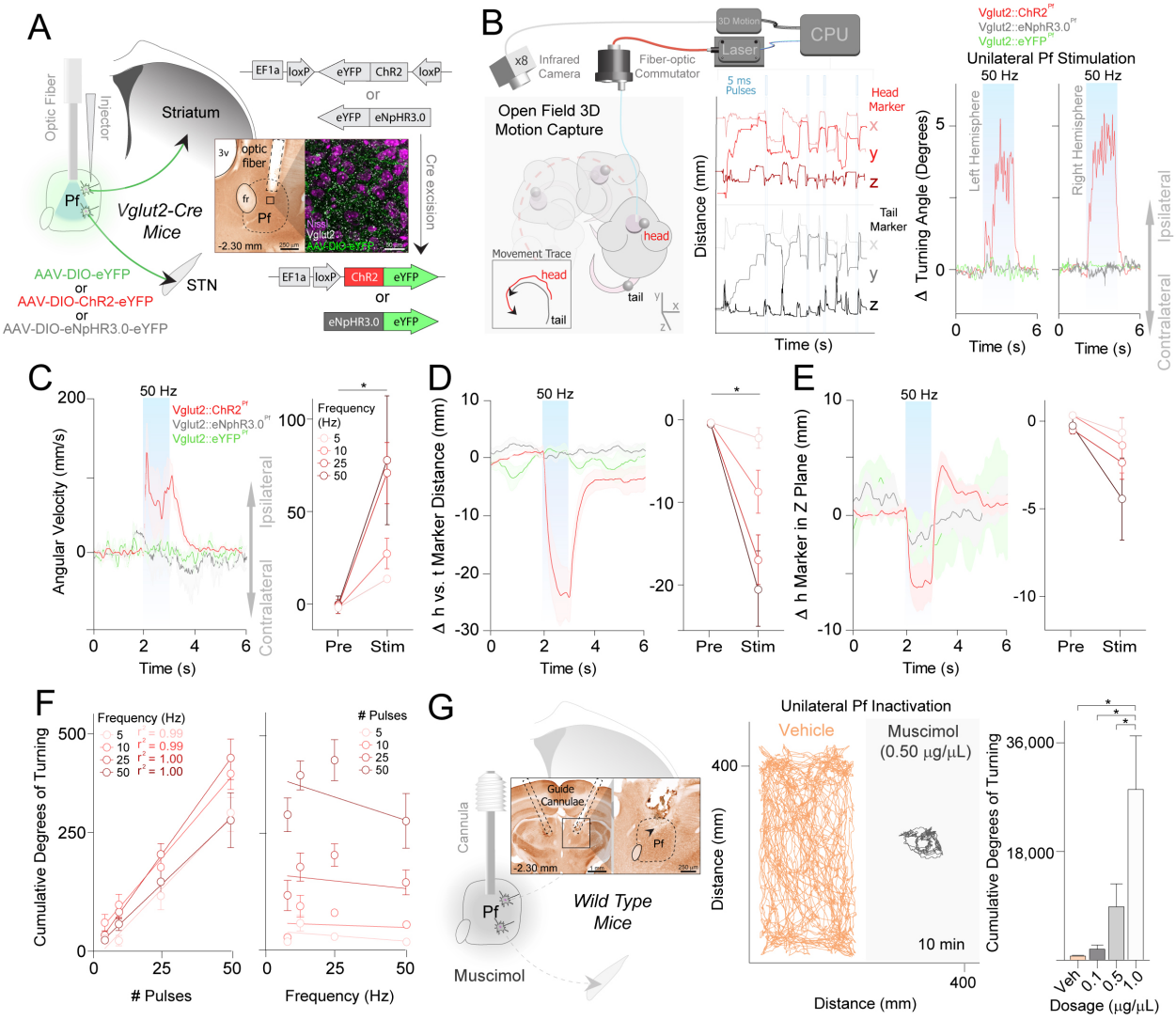

Figure 1. **Pf Excitation and pharmacological inhibition produces turning**. (**A**) Stimulation of glutamatergic neurons in the Pf (rAAV5.EF1α.DIO.hChR2(H134R).eYFP, Vglut2-Cre mice). Coronal sections through the diencephalon showing optic fiber placement above virally infected Vglut2+ neurons in the Pf. (**B**) Open-field 3D motion capture during optogenetic stimulation. Infrared cameras captured the position of reflective markers on the head and tail of mice. Unilateral excitation of Pf Vglut2+ neurons evoked ipsiversive turning (right). (**C**) Pf cell-body excitation caused a significant increase in angular velocity (two-way repeated measures ANOVA, pre vs. post stimulation ($F(1,5) = 12.46$, $p = 0.017$, $n = 6$)). (**D**) Pf cell-body excitation

caused a significant bending of the body as measured by the distance between the head and tail reflective markers (two-way repeated measures ANOVA, pre vs. post stimulation ($F(1,5) = 21.59$, $p = 0.0056$, $n = 6$)). (**E**) Pf cell-body excitation regardless of stimulation frequency did not significantly cause a lowering of the head (two-way repeated measures ANOVA, pre vs. post stimulation ($F(1,5) = 2.734$, $p = 0.16$, $n = 6$)), however post hoc analysis (Sidak's multiple comparison test) revealed a significant effect between pre-stimulation and 50 Hz excitation ($t(15) = 4.769$, $p = 0.001$) on head elevation. (**F**) Cumulative rotation in degrees significantly increased as a function of the number of stimulation pulses (left), regardless of the stimulation frequency (right) (Linear regression analyses, all $r^2 \geq .99$). (**G**) Pf muscimol inactivation through chronically implanted guide cannulae. Coronal section through the diencephalon showing cannula placement in the Pf. Representative example of movement traces after unilateral vehicle and muscimol (0.50 µg/µL) injections into the Pf (middle). Cumulative rotations in degrees significantly increased at higher muscimol dosages (right) (one-way repeated measures ANOVA, significant main effect of dosage on cumulative rotations across conditions, $F(3,28) = 6.944$, $p = 0.0012$, $n = 8$)). Post hoc comparison using Tukey's multiple comparison test indicated that the mean cumulative rotations for the 1.0 µg/µL dosage condition (M = 78.5, SD = 69.7) was significantly different from the vehicle (M = 2.0, SD = 0.93), 0.10 µg/µL (M = 5.1, SD = 5.3), and 0.50 µg/µL (M = 24.6, SD = 29.9) conditions). The 0.10 µg/µL and 0.50 µg/µL conditions were not significantly different from the vehicle condition. 3v, third ventricle.

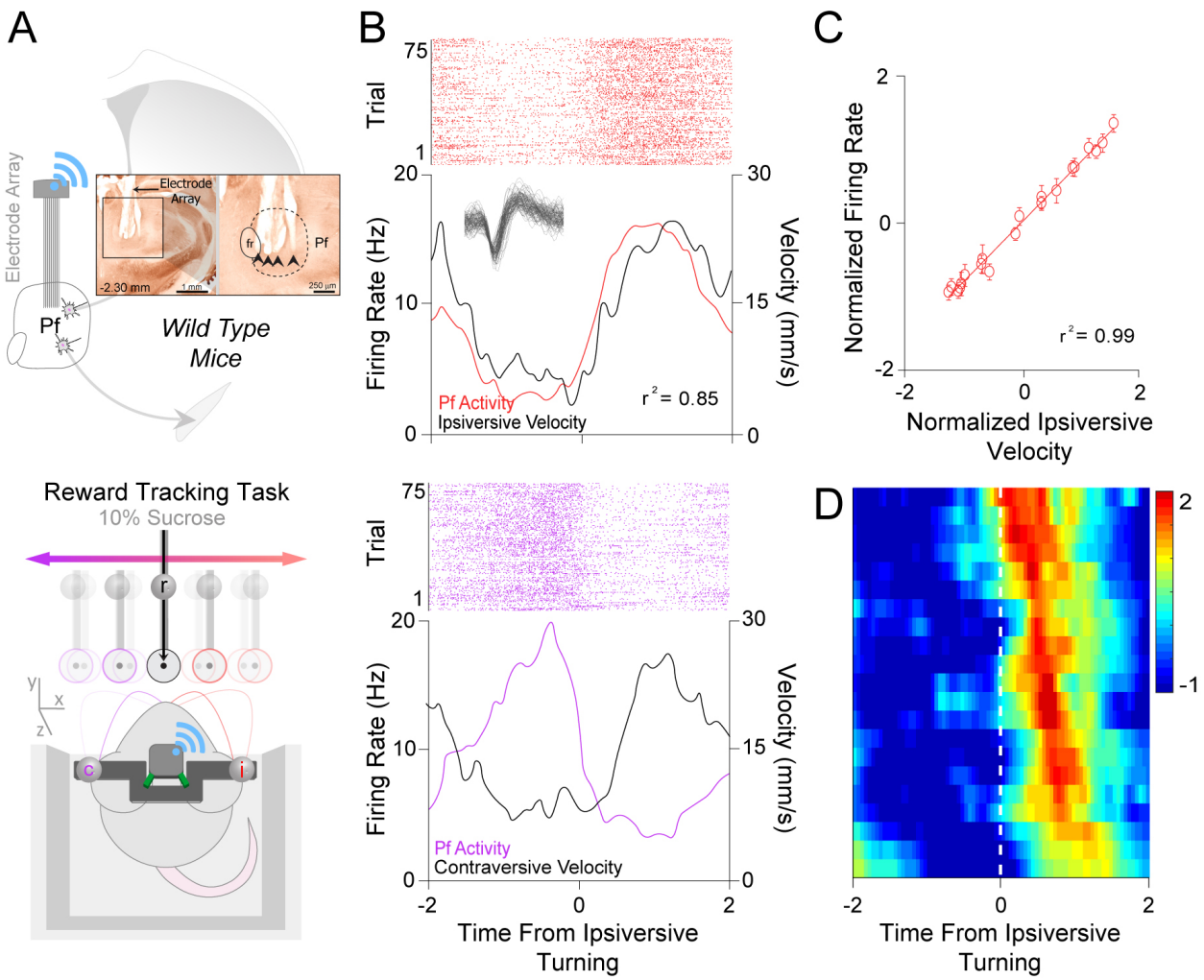

Figure 2. Neural Activity in the Pf Nucleus Encodes velocity. (**A**) Chronically implanted 16-channel electrode array into the Pf of wild-type mice. Coronal sections through the diencephalon show placement of electrode array into Pf (inset). Black arrows denote electrode tips. Pf neural activity was recorded in water deprived mice while mice tracked a moving target controlled by a stepper motor for a 10% sucrose reward (bottom). Reflective markers placed on the head (c and i) and the reward spout (r) were used to track movements in relation to the target during wireless recoding of Pf neural activity. (**B**) Peri-event histograms showing correlation of Pf neural activity with ipsiversive velocity (top) and anti-correlation with contraversive velocity (bottom) for 75 trials. (**C**) Linear regression analysis ($r^2 = 0.99$) between normalized Pf firing frequency and normalized ipsiversive velocity across Pf ipsiversive velocity-encoding neurons. (**D**) Z-scored spike density heat map. Each row represents activity from a single Pf ipsiversive velocity encoding neuron (n = 21).

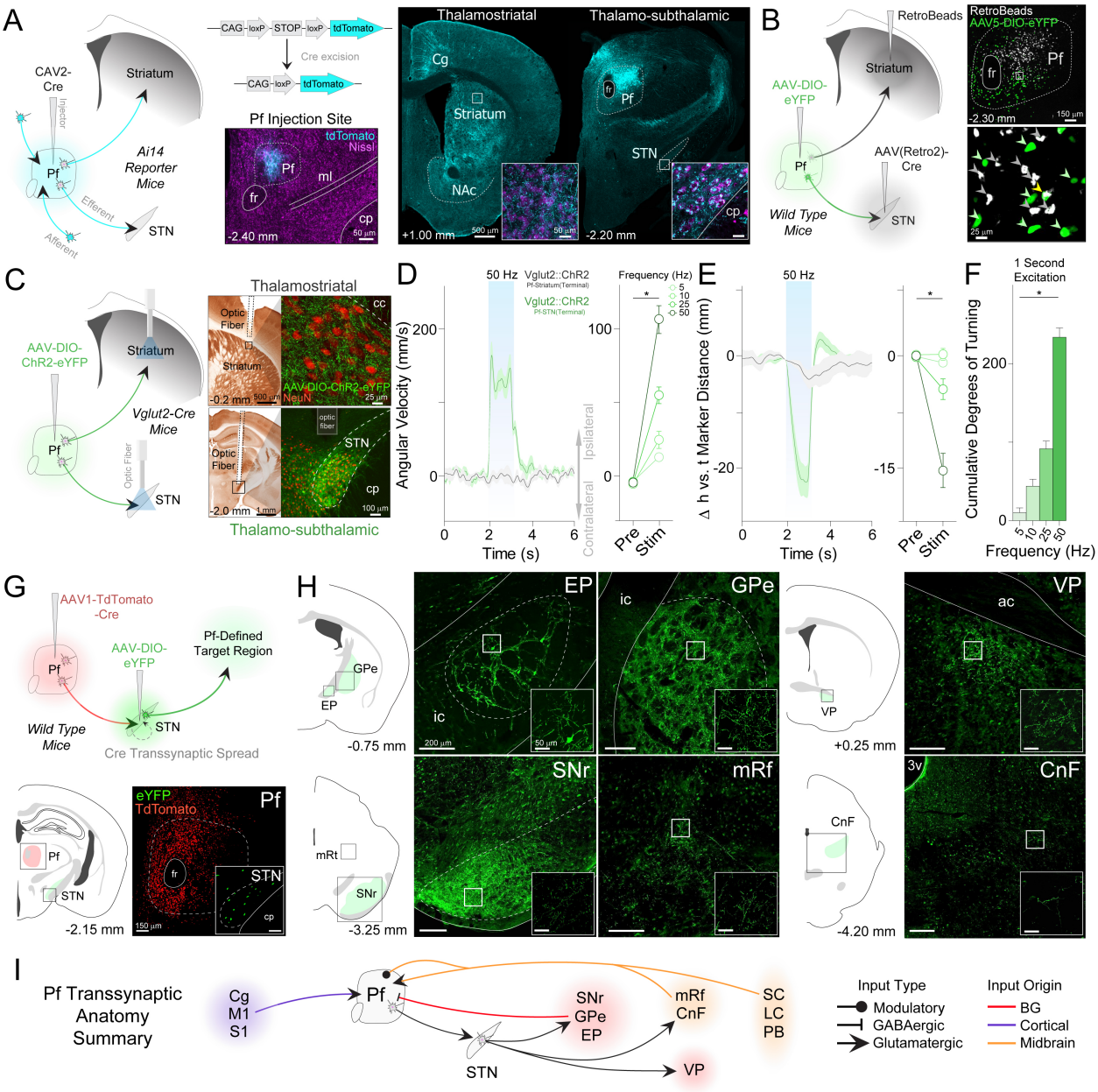

Figure 3. **Thalamo-subthalamic, but not thalamostriatal stimulation causes ipsiversive turning**. (**A**) CAV2-Cre injection into the Pf of Ai14 reporter mice to visualize input-output connectivity. Coronal sections show the Pf injection site and terminal labeling in the striatum (thalamostriatal) and STN (thalamo-subthalamic). (**B**) Coronal sections showing two distinct glutamatergic populations in the Pf revealed by dual retrograde tracing from the striatum (white)

and STN (green). Tracer colocalization shown in yellow. (**C**) Excitation of Pf infected terminals (rAAV5.EF1α.DIO.hChR2(H134R).eYFP) in the striatum (thalamostriatal) or the STN (thalamo-subthalamic) in separate cohorts of Vglut2-Cre mice. Coronal sections show optic fiber placement above Pf infected terminals in both cohorts. (**D**) Terminal excitation of Pf-STN neurons in the STN (green) caused a significant increase in angular velocity (two-way repeated measures ANOVA, pre vs. post stimulation: $F(1,7) = 62.24$, $p < .0001$, $n = 8$)). Angular velocity significantly increased as a function of frequency (right) (two-way repeated measures ANOVA, stimulation frequency ($F(3, 21) = 92.70$, $p < .0001$, $n = 8$)). (**E**) Terminal excitation of Pf-STN neurons in the STN caused a significant bending of the body as measured by the distance between the head and tail reflective markers (two-way repeated measures ANOVA, pre vs. post stimulation: $F(1,7) = 33.51$, $p = 0.0007$, $n = 8$)). No movement changes were observed during terminal excitation of Pf thalamostriatal neurons (grey). (**F**) The average cumulative rotations significantly increased during terminal excitation of Pf-STN neurons (one-way repeated measures ANOVA ($F(3,28) = 15.06$, $p < .0001$, $n = 8$)). Tukey's post hoc analysis revealed a significant difference between 5 Hz (M = 10.44, SD = 13.89 and 50 Hz (M = 233.6, SD = 103.31), 10 Hz (M = 46.38, SD = 69.01) and 50 Hz (M = 233.6, SD = 103.31) and 25 Hz (M = 91.55, SD = 68.72) and 50 Hz (M = 233.6, SD = 103.31). (**G**) Injection of AAV1.TdTomato.Cre into Pf allowed Cre transsynaptic spread into the STN. An AAV.DIO.eYFP was subsequently injected into the STN to visualize Pf-defined subthalamic projections. Coronal schematic shows Pf and STN injection sites. (**H**) Coronal sections show terminal labeling sites of Pf-defined subthalamic targets: ventral pallidum (VP), entopeduncular nucleus (EP), external segment of the globus pallidus (GPe), substantia nigra pars reticulata (SNr), mesencephalic reticular formation (mRf), cuneiform nucleus (CnF). (**I**) Summary of transsynaptic anatomy results. The Pf receives glutamatergic and modulatory input from mesencephalic brain regions. The Pf also receives inhibitory feedback from Pf-STN transsynaptic targeted BG nuclei, in addition to glutamatergic input from cortex. Tracing for additional anatomical input shown in Fig. S3. 3v, third ventricle; Cg, cingulate cortex; cp, cerebral peduncle; fr, fasciculus retroflexus; LC, locus coeruleus; M1, primary motor cortex; ml, medial lemniscus; NAc, nucleus accumbens; PB; parabrachial nucleus; S1, primary sensory cortex; SC, superior colliculus.

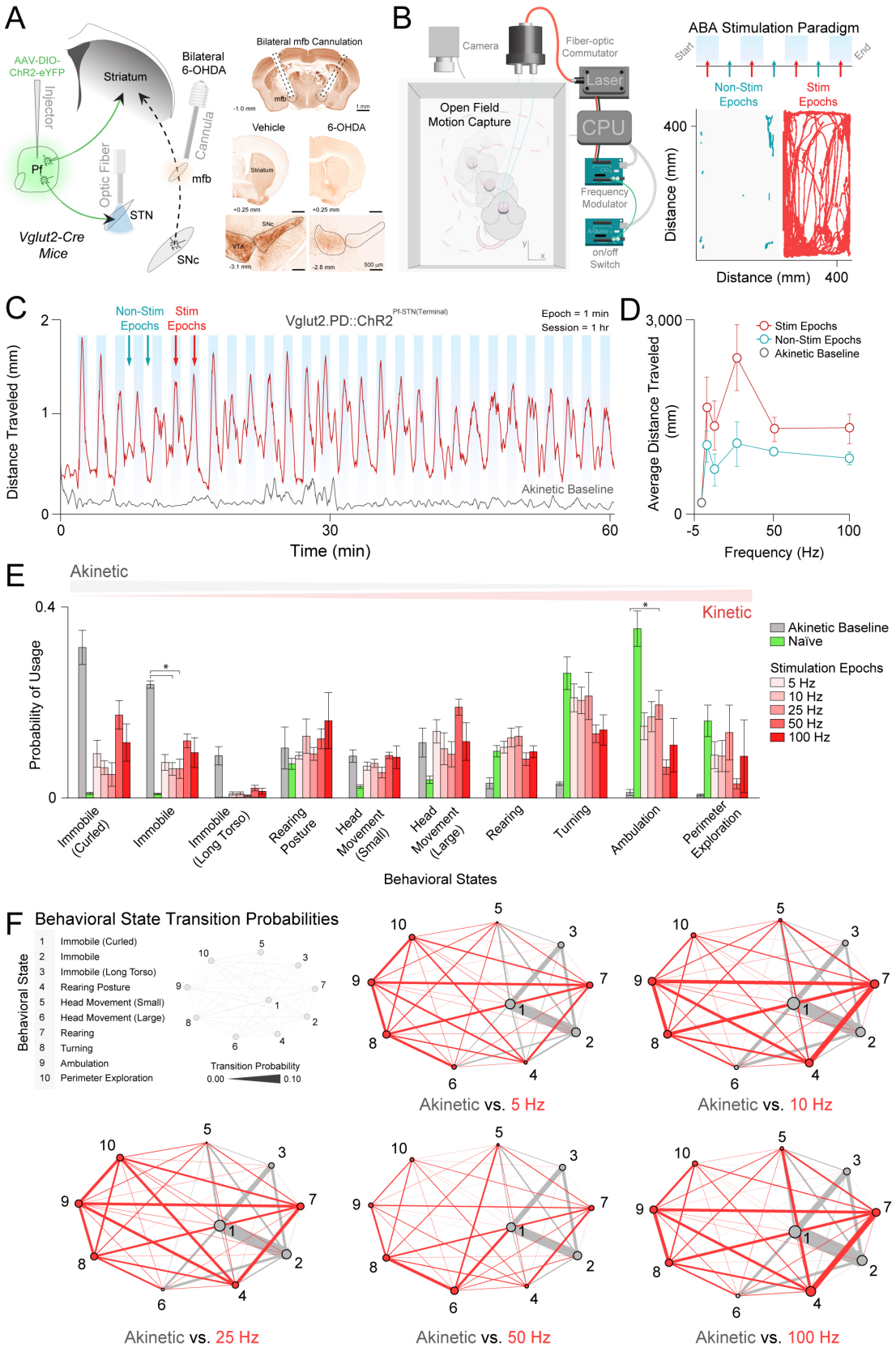

Figure 4. **Bilateral stimulation of thalamo-subthalamic terminals in the STN of bilateral-PD mice rescues akinesia and promotes movement**. (**A**) Generation of bilateral-PD mouse model by injection 6-OHDA. An injection of rAAV5.EF1α.DIO.hChR2 (H134R).eYFP was made into the Pf to excite Pf-STN terminals via an optic fiber in Vglut2-Cre mice. (**B**) Video capture of bilateral-PD mice in an open-field arena. Bilateral excitation of Pf-STN terminals in an ABA stimulation paradigm (1 min on, 1 min off) over the course of 1 hour. Representative movement traces are shown for non-stimulation and stimulation epochs for a 25 Hz stimulation session. (**C**) Representative example of ABA stimulation paradigm measuring distance traveled across 25 Hz stimulation and non-stimulation epochs. Akinetic baseline condition for same animal is also shown. **(D)** Average distance traveled. (**E**) Probability of usage of AR-HMM identified behavioral states during stimulation epochs across frequencies compared to baseline (Hotellings t-tests, $p < 0.0001$ for all comparisons except 5 Hz ($p > 0.05$)). (**F**) Bigram illustrating transition probabilities of AR-HMM defined behaviors across frequencies versus akinetic baseline and normal control. SNc, substantia nigra pars compacta.

Acknowledgements

We thank Fengxia Allen, Erin Gaidis, Xiaoran Li, Namsoo Kim, and Murray Wickwire for technical assistance, and Michael Tadross and Nicole Calakos for helpful comments on the manuscript. **Funding:** This work was supported by grants NS094754 and MH112883 to HHY.
Author contributions: G.D.R.W. and H.H.Y. conceptualized and designed studies. G.D.R.W. and R.N.H performed surgeries, behavioral experiments, and electrophysiological recordings. G.D.R.W. performed immunohistochemistry, confocal imaging, and supervised all experiments. E.A.P. wrote data collection and analysis code, ran the Autoregressive Hidden Markov Model, and analyzed the output data. G.D.R.W. and H.H.Y. drafted the manuscript. All authors analyzed data and performed statistical analyses. All authors have read and approved the manuscript. **Competing interests:** The authors report no biomedical financial interests or potential conflicts of interest. **Data and materials availability:** All data are available in the main text or the supplementary materials. Raw data available upon request from corresponding author.

Supplementary Materials

Materials and Methods

Fig S1 – S5

Movies S1-S7

Materials and Methods

All experimental procedures were conducted in accordance with standard ethical guidelines and were approved by the Duke University Institutional Animal Care and Use Committee.

Contact for Reagents and Resource Sharing

Further information and requests for resources and reagents should be directed to the corresponding author, Henry H. Yin (hy43@duke.edu).

Experimental and Subject Details

All behavioral data were collected from wild-type (C57BL/6J, Jackson labs) and Vglut2-ires-Cre mice (Slc17a6$^{tm2(cre)Lowl}$, Jackson labs). Vglut2-ires-Cre mice have Cre-recombinase expression under the control of Vglut2 receptor regulatory elements without disrupting endogenous vesicular glutamate transporter 2 expression. Optogenetic control of Pf glutamatergic neurons was achieved with a double-floxed inverted recombinant AAV5 virus injection to express either the excitatory opsin ChR2-eYFP, or the inhibitory opsin eNpHR3.0-eYFP in Vglut2+ Pf neurons. Viral infection in the Pf was histologically verified with eYFP imaging colocalized against a Vglut2 antibody and Fluoro Nissl staining (Fig. 1A). Wild-type mice were used for Pf muscimol inactivation, retrograde tracing, pathway-specific retrograde Cre expression, and transsynaptic tracing experiments. Conventional anatomical tracing data was collected from Ai14 reporter mice (129S6-Gt(ROSA)26Sor$^{tm14(CAG-tdTomato)Hze}$/J, Jackson labs). Ai14 reporter mice harbor a loxP-flanked STOP cassette that is excised in the presence of Cre to promote transcription of a CAG promoter-driven red fluorescent protein variant (tdTomato). For bilateral-PD experiments, Vglut2-ires-Cre mice were used for Pf-STN terminal excitation experiments and wild-type mice were used for Pf-STN cell-body excitation experiments.

Viral Constructs

CAV2-Cre was obtained from Institut de Génétique Moléculaire de Montpellier. AAV5.Syn.Chronos.GFP.WPRE.bGH was obtained from the University of Pennsylvania Vector Core. RAAV5.EF1α.DIO.hChR2(H134R).eYFP, rAAV5.EF1α.DIO.eNpHR3.0.eYFP, rAAV5.EF1α.DIO.eYFP, AAV1.hSyn.tdTomato.Cre, and AAV(retro2).hSyn.EF1α.Cre.WPRE were obtained from the Duke University Vector Core.

Mice were anesthetized with 2.0 to 3.0% isoflurane mixed with 0.60 L/min of oxygen for surgical procedures and placed into a stereotactic frame (David Kopf Instruments, Tujunga, CA). Meloxicam (2 mg/kg) and bupivacaine (0.20 mL) were administered prior to incision. To optogenetically interrogate Pf, adult Vglut2-IRES-Cre mice were randomly assigned to Vglut2::ChR2^{Pf} (n = 4, 2 males, 2 females, 8-10 weeks old), Vglut2::eNpHR3.0^{Pf} (n = 4, 2 males, 2 females, 8-10 weeks old), or Vglut2::eYFP^{Pf} groups (n = 4, 2 males, 2 females, 8-10 weeks old). Craniotomies were made bilaterally above the Pf and virus was microinjected through a pulled glass pipette at various penetrations and depths (0.6 μL each hemisphere, AP: -2.10 – 2.50 mm relative to bregma, ML: ± 0.60 – 0.75 mm relative to bregma, DV: -3.70 – 3.10 mm from skull surface) using a microinjector (Nanoject 3000, Drummond Scientific). Wild-type mice were used to selectively target Pf thalamostriatal (n = 4, 2 males, 2 females, 8-10 weeks old) and thalamo-subthalamic (n = 4, 2 males, 2 females, 8-10 weeks old) neurons by bilaterally injecting AAV(retro2).hSyn.EF1α.Cre.WPRE into the entire rostrocaudal and mediolateral extent of the striatum (1 μL each hemisphere, AP: +1.35 – -0.75 mm relative to bregma, ML: ± 1 – 2.75 mm relative to bregma, DV: 2.0 – 3.50 mm from skull surface) or the STN (AP: -1.90 – -2.20 mm relative to bregma, ML: ± 1.40 – 1.80 mm relative to bregma, DV: 4.10 – 4.40 mm from skull surface) in parallel with a Cre-dependent ChR2 virus injected into the Pf nucleus. For Pf cell-body stimulation, custom-made optic fibers (5-6 mm length below ferrule, >80% transmittance, 105-mm core diameter) were implanted directly above the nucleus (AP: -2.30 mm relative to bregma, ML: ± 1.20 – 1.30 mm relative to bregma, DV: 2.70 – 2.80 mm from skull surface, 10°). Thalamo-subthalamic terminals from the Pf were targeted with optic fibers implanted directly above the STN (AP: -1.80 – 2.0 relative to bregma, ML: ± 1.50 – 1.60 mm relative to bregma, DV: 4.20 mm from skull surface). For conventional anatomy experiments (n = 3, 2 males, 1 female, 8-10 weeks old), 15-20nL of CAV2-Cre or 75-100 nL or Red Retrobeads (Lumafluor Inc.) was injected at one depth to prevent leakage. For transsynaptic tracing

experiments (*n* = 3, 1 male, 2 females, 8-10 weeks old), AAV1.hSyn.tdTomato.Cre was injected into the Pf and rAAV5-EF1α-DIO-eYFP was injected into the STN using the coordinates previously listed. For all virus injections, the pipette sat at the last injection depth of each penetration for 10 minutes before being withdrawn from the brain to facilitate uptake. To pharmacologically inactivate the Pf nucleus, muscimol was injected in adult wild-type mice (*n* = 5, 2 males, 3 females, 10-12 weeks old) through 15-gauge (5 mm length) guide cannulae (Plastics One) positioned above Pf at an angle (AP: -2.30 mm relative to bregma, ML: ± 1.20 - 1.30 mm relative to bregma, DV: 2.60 - 2.80 mm from skull surface, 25°). Bilateral-PD mice (*n* = 5, 3 males, 2 females, 8-10 weeks old) were generated by implanting 15-gauge (7 mm length) guide cannulae implanted above the mfb (AP: -0.95 mm relative to bregma, ML: ± 3.10 mm relative to bregma, DV: 4.10 mm from skull surface, 25°). For electrophysiology experiments (*n* = 6, 3 males, 3 females, 8-10 weeks old), a prefabricated 4x4 electrode array (Innovative Neurophysiology, 150 µm electrode and row spacing) was lowered into the Pf (AP: -2.30 mm relative to bregma, ML: ± 0.65 mm relative to bregma, DV: 3.30 mm from skull surface) at a rate of 300 µm/min. All fibers and cannulae were secured in place with dental acrylic adhered to skull screws. Mice were group housed and allowed to recover for one week before experimentation.

Optogenetic Stimulation and 3D Motion Tracking

For 3D motion capture experiments, mice were connected to a 473-nm DPSS laser (Shanghai Laser) for optogenetic excitation and a 589-nm DPSS laser for optogenetic inhibition experiments via fiber optic cables (105/22A, Precision Fiber) in a square open field arena (22" L, 22" W, 1" H) elevated 3'. The output from each sheathed optic fiber tip was measured (PM120VA, ThorLabs) before each experimental session to obtain a power between 9-10 mW (i.e. ~8mW power delivered to the stimulation site with a transmittance of ~85%). A Matlab program interfaced to a National Instruments Box triggered a 5 ms square pulse at varying frequencies (5 - 100 Hz) and durations (50 ms - 20 s). Movements at a millimeter spatial resolution were captured in a Cartesian plane with eight Raptor-H digital infrared cameras (Motion Analysis, CA, 100 Hz sampling rate). The cameras were placed equidistantly around the arena where two reflective spherical markers (6.35 mm diameter) that were located on both the fiber sleeve and tail of the mouse could be recorded. Cameras were calibrated before each

experimental session. The output of the laser was channeled through an optic patch cable connected to a commutator above the open field arena. A rotating optical commutator (Doric) divided the beam (50:50) permitting bilateral stimulation. Stimulation was triggered randomly during a 12 to 15 second interval after cessation of the previous stimulation trial using a custom Matlab script to prevent mice from predicting the stimulation onset. Stimulation parameters were consistent within a session, but the order of stimulation (i.e., frequency and duration) was semi-randomized between mice. Unilateral and bilateral stimulation data were taken from the same animals. For unilateral experiments, separate stimulation data sessions were acquired from each hemisphere of the same animal on separate days.

Pharmacological Inactivation and Medial Forebrain Bundle Lesion

Muscimol inactivation experiments were conducted on wild-type mice 10 days after cannulation surgery. Before each muscimol injection, a 10-minute baseline video was taken. All mice were anesthetized with 2.5% isoflurane and a 33-gauge injector was inserted through the cannula that extended 500 μm beyond the cannula tip. Varying dosages of muscimol (0.1, 0.5, and 1.0 μg/μL) or vehicle (0.9% saline) were unilaterally injected using a custom microinjector and microinfusion pump (PHD 2000, Harvard Apparatus) at a rate of 100 nL/min for 2 min. The injector was withdrawn after 10 minutes to allow sufficient uptake of the drug. Mice were then placed in the center of a rectangular open field arena (17.5" L, 9.5" W, 6.25" H) before recording video of movement 15 min post-injection. An open source software program (Bonsai) using a custom script tracked movements for 10 min (*27*). Two-dimensional coordinates based on the center of mass of each mouse were collected at 30 f/s. Because muscimol has a relatively short half-life (~ 6 hrs), dosage response experiments were conducted 24 hrs apart in a randomized fashion, resulting in a total of 4 injections per hemisphere for each mouse. The same injection procedures were followed to generate bilateral-PD mice using 6-OHDA (2.0 mg, 1300 nL/hemisphere). A baseline video (50 f/s) was taken 3 days after 6-OHDA injections in a rectangular open field arena (19" L, 10" W, 12" H). An ABA stimulation paradigm was then used to optogenetically excite Pf-STN neurons in bilateral-PD mice over 1 hour across various frequencies (5, 10, 25, 50, and 100 Hz). To achieve short latency control of the laser, we used two Arduinos. The first Arduino served as a data acquisition device to receive digital output signals from the computer. The second Arduino modulated frequency output from the laser

using TTL pulses. Stimulation conditions and equipment were the same as previously described for 3D tracking experiments. One-minute stimulation and non-stimulation epochs were interleaved to comprise a total duration of 30 minutes for each epoch during a session. Mice were allowed to rest 3 hours between stimulation sessions to prevent any movement rescue effect contamination from the previous session.

3D Motion Tracking Analysis

A custom Matlab script pre-processed data smoothed at 6 Hz from Cortex 3D movement tracking acquisition software (Motion Analysis) to output movement kinematic information in Neuroexplorer with respect to stimulation timestamps. Peri-event histograms and rasters were generated in Neuroexplorer and analyzed in GraphPad Prism. Angular Velocity kinematic data was binned at 25 ms and the mean and SEM for each bin across experimental animals was computed to produce movement traces. Kinematic data for head and tail marker distance, head in the z plane, as well as forward velocity were standardized by a Z-score transformation to standardize measurements across animals. Angular Velocity was not standardized due to similar velocity profiles across animals. All kinematic statistical analyses were performed on the one second of data preceding stimulation compared to the one second of stimulation data.

Wireless *in vivo* Electrophysiology Recordings

A 128-Channel neural signal data acquisition system (Cerebus, Blackrock Microsystems) recorded action potentials through a miniaturized wireless headstage (Triangle Biosystems) interfaced to manufactured electrode arrays (Innovative Neurophysiology). Data were filtered with both analog and digital bandpass filters before being sampled as previously described(8). Collected neural data was sorted offline with OfflineSorter (Plexon) and analyzed in Neuroexplorer (Nexus). Discharges with a signal-to-noise ratio of a least 3:1 were time-stamped at a resolution of 0.1 ms. Waveforms were classified as single units using the following criteria: 1) a signal to noise ratio of at least 3:1; 2) consistent waveforms throughout the recording session; 3) refractory period of at least 800 μs.

Tracking Task Design and Data Analysis

Pf neural activity was recorded in water deprived mice while mice tracked a moving target

controlled by a stepper motor to receive a 10% sucrose reward at 2.7 μL/s (Bipolar, 56.3 x 56.3 mm, DC 1.4A, 2.9 Ω, 1.8 degrees/step, Oriental Motor, USA). The stepper motor was controlled by a custom Matlab script and programmed to traverse a total horizontal distance of 120 mm. One infrared marker placed 20 mm from the sucrose spout and two markers placed on each side of a custom printed head bar were used to track head movements in relation to the target. Electrophysiology recordings were processed as described in the previous section. Matlab communicated with Cortex program online to control reward delivery every 500 ms if the mouse tracked the target for a duration greater than 1 s. The tracking threshold was defined as the center of the head within 50 mm in the x plane and 30 mm in the y plane of the target marker. Prior to recording sessions, mice were trained until they tracked the target consistently (~1 hour of training over four days). Mice were first trained to track a target moving at a constant speed (16mm/s). The speed of the target was then varied randomly during recording sessions (5-48 mm/s) and updated every 2 ms by Matlab. Self-rightward and -leftward movement were defined as movement to start the respective direction at least over 1 s. For linear regression analysis of single unit activity and behavioral variables, both neural data captured at 30 Hz and behavioral data captured at 100 Hz were split into 50 ms bins within a timeframe of 5 s in Neuroexplorer. Output data were exported into GraphPad Prism, where a linear regression analysis was performed. For population analyses, neural data and behavioral variables binned at 250 ms were standardized by a Z-score transformation within each session in Matlab. The transformed data from each animal were then averaged together to get a population Z-score for both the behavioral variables and the neural data. Once these Z-scores were obtained, the data were exported into GraphPad Prism, where a linear regression analysis was performed.

Continuous behavioral classification

An unsupervised classification method was used to systematically and continuously measure behavior in pharmacological inactivation and PD optogenetic experiments. Animals were placed in an open-field arena and filmed with a camera positioned 0.7 meters from the floor of the arena. Data was recorded on a Dell computer (16GB RAM, Intel i7, 1TB SSD) via a 2.0 USB adaptor at 50 frames/s. A region of interest was outlined and all further preprocessing was performed on the cropped image in Python using scientific tools and open source packages. Specifically, a binary threshold was applied to each frame of the video, and a 100x100 pixel

frame was cropped around the animal. Each frame was then aligned (https://github.com/gordonberman/MotionMapper) to eliminate allocentric components of behavior (*28*). Following the extraction and alignment of the mouse's image, a wavelet decomposition was applied to increase the dimensionality of the image for better classification of postural dynamics. Next, a principal components analysis was performed to reduce the dimensionality to the top 10 principal components. Reducing the dimensionality provided data that was easier to feed into an autoregressive hidden Markov model (AR-HMM)(*17*). The AR-HMM model takes into account the image of the mouse, the duration of the specific behavioral 'syllable,' and the transition probabilities to other syllables. Specifically, using Gibbs sampling with an AR-HMM will segment all of the data into distinct behavioral states, and then switch to update these segments and the transitions between them (*28*). Each model goes through 1,000 iterations of Gibbs sampling. Importantly, all data (i.e. all groups) was co-trained to compare behavioral states across conditions. The output of the AR-HMM model allows behavioral classification into modules that occur systematically, thereby assigning behavior a syntactic structure similar to language. Each video frame was assigned a behavioral label, which was used to calculate the probabilities of using each behavioral state, as well as the probabilities of transitioning between states. Following the model output, additional statistical analyses were conducted. For each mouse, bootstrapped samples were computed to assess significance in module usage, as well as transition probabilities. Group comparisons were achieved with the Hotelling t-squared statistic. To assess individual differences between behavioral states, we estimated the variance of the data through bootstrapping. Using the bootstrapped estimates of variance, we performed a wald-test. We corrected for multiple comparisons using the Holm-Bonferonni method. Visualization of the data was also conducted in Python to create videos (OpenCV), graphs (networkx), and plots (matplotlib).

Behavioral State Probability

Behavioral states were classified using an AR-HMM. Videos of the states were created and specific behaviors were characterized for the top 10 mostly commonly observed behaviors. Here the probabilities of displaying each behavior are sorted by usage across all groups. The probability of each behavior is displayed separately for each group.

Transition analysis

This analysis examines the probability of transitioning between different behavioral states. Here the probability of using certain behaviors is displayed in the size of the nodes. The probability of transitioning between behaviors is represented by the thickness of the lines. Positions of the states are kept constant across all three panels. Initial positions are seeded using a spring algorithm, where the probability of transferring between behaviors determines the spacing of the nodes. Nodes naturally repel each other. Each connection acts like a spring pulling together nodes with strength proportional to transition probability. The behavioral usage and transition probabilities were subtracted from each other, so that the remaining images represent the differences in probabilities between groups.

Histology and Immunohistochemistry

Mice were deeply anesthetized and perfused with 0.1M PBS containing heparin followed by 4% paraformaldehyde after completion of experimentation. For mice with fiber and cannulae implants, heads were stored in 4% paraformaldehyde with 30% sucrose for 24-48 hrs at 4 ºC to aid histological verification of placement. Brains were fixed in 30% sucrose thereafter. After sinking, brains were sliced coronally at 60 μm using a Leica CM1850 cryostat.

For optogenetic experiments, the first 1-in-2 series of sections was processed for the presence of cytochrome oxidase to visualize cytoarchitecture. Briefly, sections were rinsed in 0.1M PB before incubating in a diaminobenzidine (DAB), cytochrome C, and sucrose solution for ~2 hours at room temperature. The second series of sections was processed to enhance eYFP labeling. Sections were rinsed in 0.1M PBS for 20 min before being placed in a PBS-based blocking solution containing 5% goat serum and 0.25% Triton X-100 at room temperature for 1 hr. Sections were then incubated with a primary antibody (polyclonal chicken anti-GFP; 1:500 dilution; Abcam; catalog no. ab13970) in blocking solution overnight at 4 °C. Sections were then rinsed in PBS for 20 min before being placed in a secondary antibody used to visualize ChR2 as marked by YFP colocalization (goat anti-chicken Alexa Fluor 488; 1:1000 dilution; ThermoFisher; catalog no. A-11039) for 1 hr at room temperature. Fiber placement and injection site visualization was further aided by Fluoro Nissl (1:200 dilution; Molecular Probes; catalog no. N21479) staining for 20 minutes at room temperature, or with the neuronal marker NeuN (monoclonal rabbit anti-NeuN; 1:1000 dilution; Abcam; catalog no. ab177487).

For anatomical experiments, the endogenous signal caused by CAV2-Cre injection into Ai14 mice or retrobead injections into wild-type mice was not enhanced. Primary antibodies for choline acetyltransferase (monoclonal rabbit anti-choline acetyltransferase; 1:1000 dilution; Abcam; catalog no. ab178850) and noradrenaline (polyclonal rabbit anti-noadrenaline; 1:500 dilution; Abcam; catalog no. ab8887) were used to identify neuronal subtype as marked by colocalization with tdTomato in the brainstem (goat anti-rabbit Alexa Fluor 488; 1:1000 dilution; Abcam; catalog no. ab150077) using the immunohistochemistry protocol previously described for eYFP enhancement.

Cytochrome oxidase sections were dehydrated in 200 proof ethanol, defatted in xylene, and coverslipped with cytoseal. Sections for fluorescent microscopy were mounted and immediately coverslipped with Fluoromount aqueous mounting medium (Sigma; catalog no. F4680). Brightfield images were acquired and stitched using an Axio Imager.M1 upright microscope (Zeiss) and fluorescent images were acquired and stitched using a Z10 inverted microscope (Zeiss). Confirmation of optical fiber placement was performed by comparing images with a mouse brain atlas (*29*).

Tyrosine Hydroxylase Processing and Quantification

A Tyrosine hydroxylase reaction was performed to visualize pallidal and striatal dopaminergic cell death in 6-OHDA injected mice. Briefly, sections were first agitated in a 3% H_2O_2 solution for 10 min at room temperature to block endogenous peroxidases. Sections were then transferred to a PBS-based blocking solution containing 5% goat serum and 0.25% Triton X-100 at room temperature for 1 hr. After incubating overnight in blocking solution containing a primary antibody (polyclonal rabbit anti-tyrosine hydroxylase; 1:1000 dilution; Millipore; catalog no. 657012), sections were incubated for 1 hr at room temperature in a biotinylated solution (biotinylated goat anti-rabbit IgG; 1:200 dilution; Vector Laboratories; catalog no. BA-1000) before incubating in an avidin-biotin horseradish peroxidase solution for 2 hrs at room temperature (Vector Novoxastra Laboratories). After rinsing sections in PBS, Tyrosine hydroxylase neurons were visualized with 0.05% DAB and 0.005% H_2O_2 in double distilled H_2O, pH 7.2, for 5-10 min. The DAB reaction was stopped with subsequent PBS washes and stored at 4 °C. Tyrosine hydroxylase-reacted sections were dehydrated in 200 proof ethanol, defatted in xylene, and coverslipped with cytoseal. The intensity of tyrosine hydroxylase staining

in saline injected (n = 3) and experimental groups (n = 12) was quantified as previously described (*19*). Bilateral-PD animals were included in analyses if tyrosine hydroxylase intensity values were <80% compared to controls. Two bilateral-PD animals were excluded from the study because they did not meet this criterion.

Quantification and Statistical Analysis

The values and error bars reported in the text are the mean ± SEM, respectively. Behavioral data was analyzed with MATLAB 2015b (MathWorks). Statistical tests were performed in Prism 5 (GraphPad). Two-tailed parametric tests were used. An a priori alpha level of 0.05 was used to determine significance.

Supplementary Figures

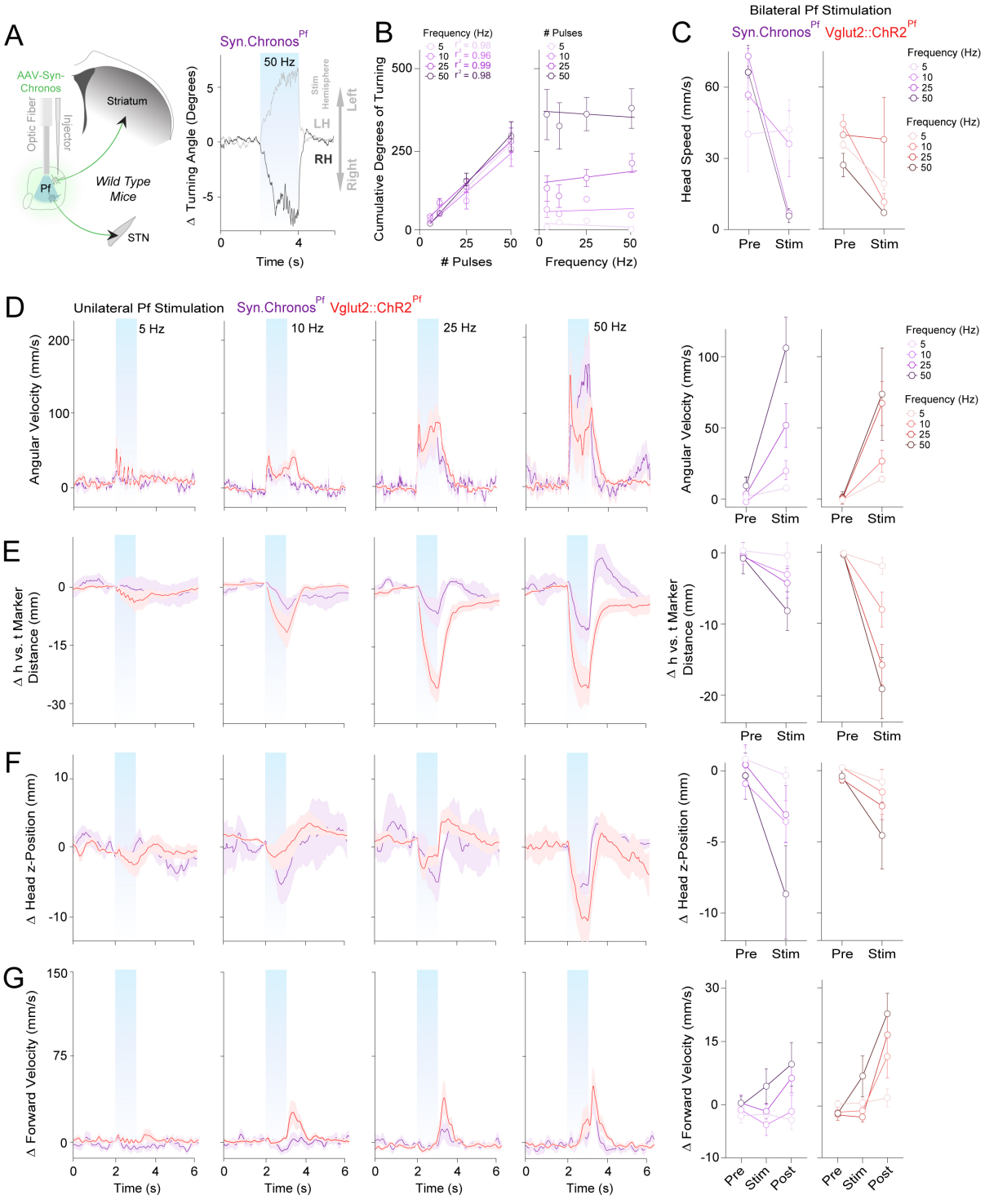

Supplementary Figure 1. **Pf Excitation causes ipsiversive turning and related movement kinematic changes across stimulation frequencies**. (**A**) Excitation of Pf virally-infected neurons after injection of AAV5.Syn.Chronos-GFP.WPRE.bGH. (**B**) Change in turning angle

after ipsilateral excitation of Syn.Chronos infected neurons in the Pf. Average degrees of cumulative rotations increased as a function of frequency and the number of pulses. (**C**) Changes in head speed during optogenetic stimulation of Syn.Chronos and Vglut2::ChR2 neurons in the Pf across various frequencies. Head speed is significantly decreased due to stimulation in Syn.Chronos animals (two-way repeated measures ANOVA ($F(1,2) = 493.9$, $p = 0.002$, $n = 3$). There was no significant decrease in Vglut2::ChR2 animals (two-way repeated measures ANOVA ($F(1,2) = 7.617$, $p = 0.11$)). (**D**) Unilateral excitation of Pf significantly increased angular velocity in Syn.Chronos (two-way repeated measures ANOVA ($F(1,6) = 16.68$, $p = 0.0065$, $n = 7$)) and Vglut2::ChR2 (two-way repeated measures ANOVA ($F(1,5) = 12.46$, $p = 0.0167$, $n = 6$)) animals across various frequencies. (**E**) Unilateral excitation of Pf caused a significant bending of the body in Syn.Chronos (two-way repeated measures ANOVA ($F(1,6) = 16.62$, $p = 0.0065$, $n = 7$)) and Vglut2::ChR2 (two-way repeated measures ANOVA ($F(1,5) = 21.59$, $p = 0.0056$, $n = 6$)) animals. (**F**) Unilateral excitation of Pf caused a significant head e in Syn.Chronos animals (two-way repeated measures ANOVA ($F(1,6) = 9.617$, $p = 0.0211$, $n = 7$)). There was no significant effect in Vglut2::ChR2 animals (two-way repeated measures ANOVA ($F(1,5) = 21.59$, $p = 0.0056$, $n = 6$)), however Sidak's post hoc multiple comparison test revealed a significant difference between pre-stimulation and the 50 Hz condition ($t(15) = 4.69$, $p = 0.0010$)).

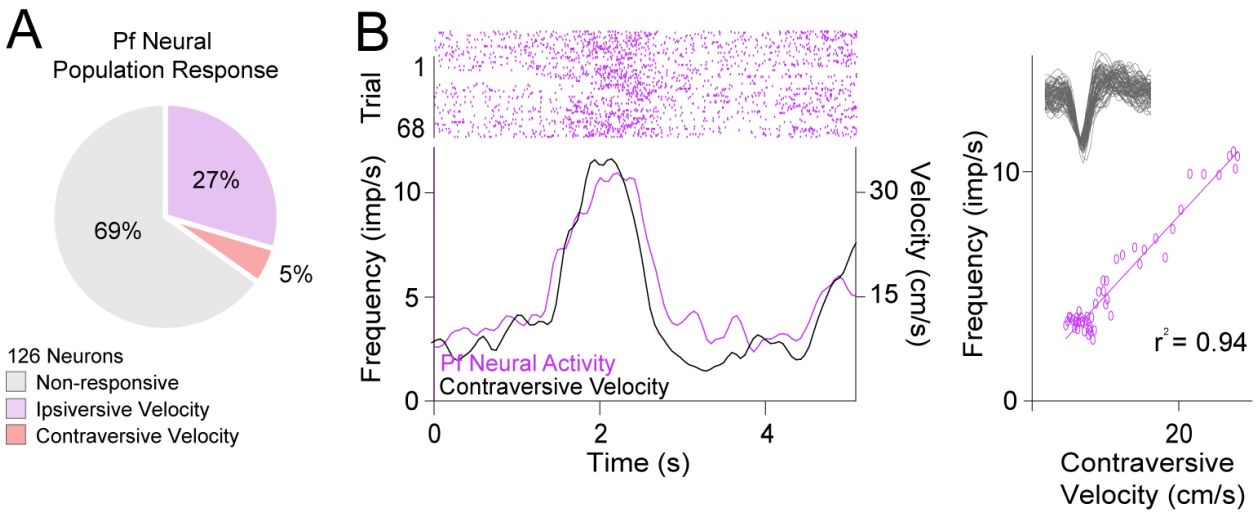

Supplementary Figure 2. **A subset of Pf neurons encode contraversive velocity**. (**A**) Pf

neural population response (n = 126). (**B**) Peri-event histogram showing example of contraversive encoding neuron in Pf (left). Linear regression analysis ($r^2 = 0.94$) of Pf firing frequency and contraversive velocity of representative neuron.

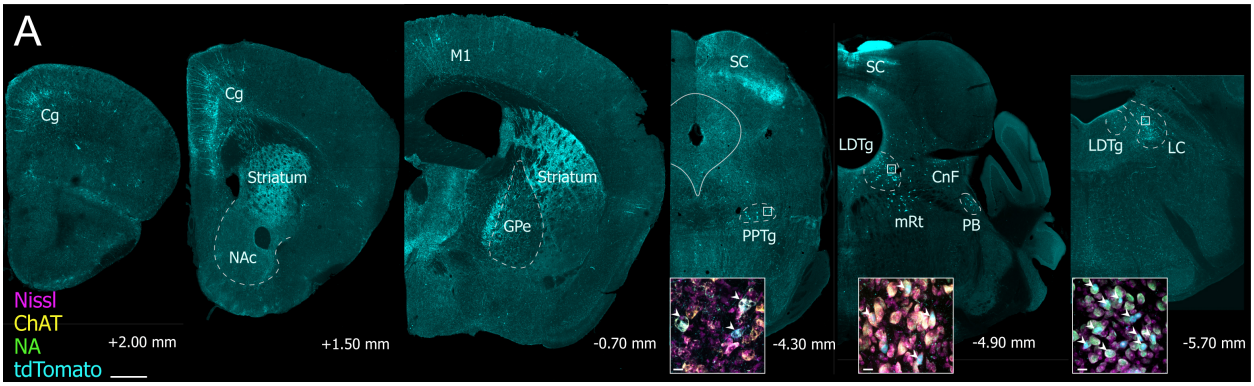

Supplementary Figure 3. **The Pf nucleus interacts with basal ganglia nuclei and brainstem nuclei of the reticular activating system.** (**A**) Input-output projections from CAV2-Cre injection into the Pf shown in Figure 3. Series of coronal sections through the levels of the basal ganglia and mesencephalon. Insets show retrograde-labeled neurons in neuromodulatory areas of the mesencephalon. White arrows denote colocalization. Abbreviations; Cg, cingulate cortex; ChAT, choline acetyltransferase; CnF, cuneiform; GPe, external globus pallidus; LC, locus coeruleus; LDTg, laterodorsal tegmentum; M1, primary motor cortex; mRt, mesencephalic reticular formation; NA, noradrenaline; NAc, nucleus accumbens; PB, parabrachial nucleus; PPTg, pedunculopontine tegmentum; SC, superior colliculus.

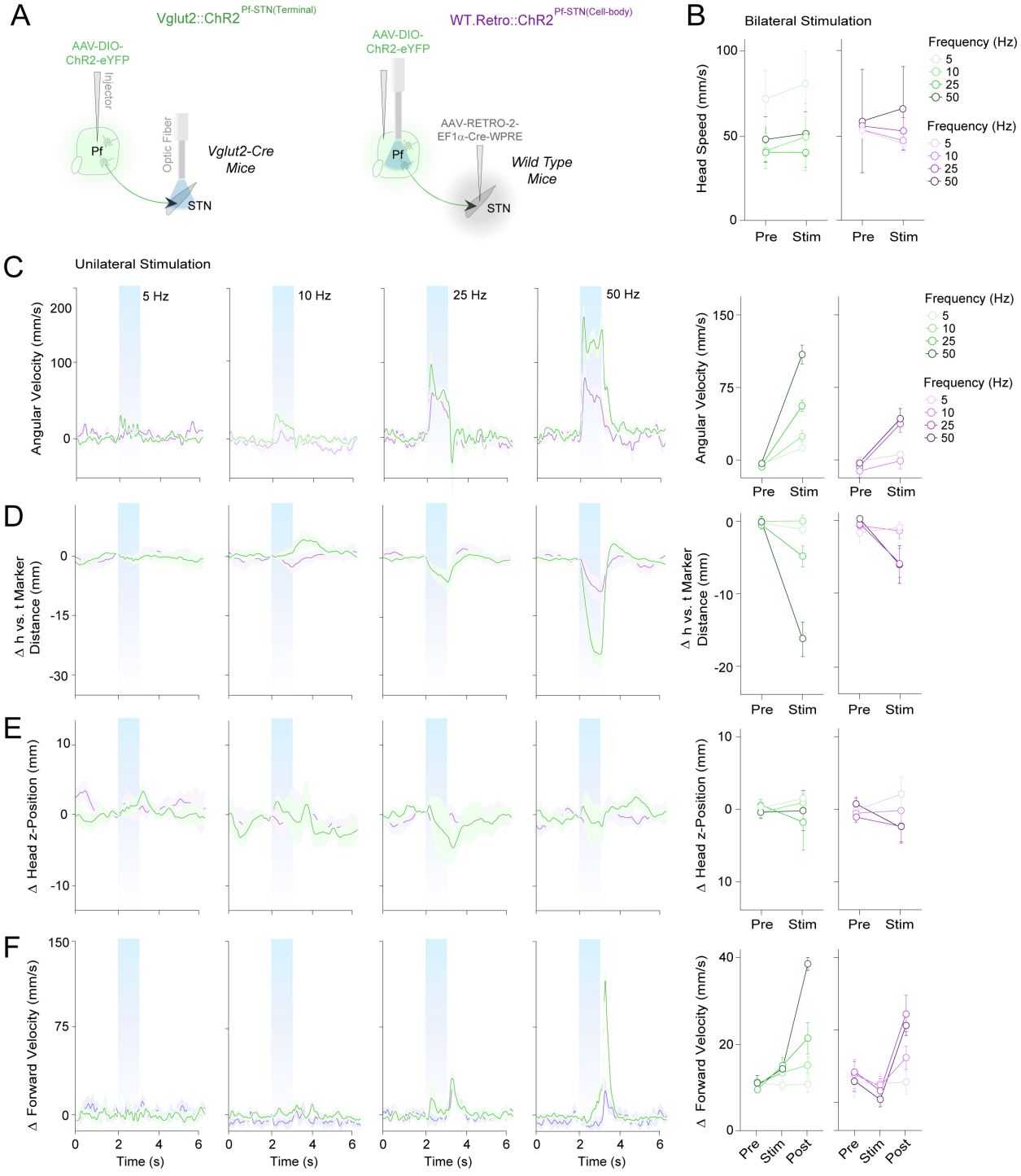

Supplementary Figure 4. **Excitation of Pf-STN neurons evokes ipsiversive turning across stimulation frequencies**. (**A**) Terminal excitation of Pf-STN virally infected neurons after injection of rAAV5.EF1.DIO.hChR2(H134R).eYFP (left) and retrograde soma stimulation of Pf-STN neurons after injection of AAV(retro2).hSyn.EF1α.Cre.WPRE and rAAV5.EF1.DIO.hChR2(H134R).eYFP (right). (**B**) Change in head velocity after bilateral Pf terminal stimulation in the STN and soma excitation of Pf-STN neurons. Terminal Pf-STN stimulation produced a significant increase in head velocity (two-way repeated measures ANOVA ($F(1,2) = 493.90$, $p = 0.002$, $n = 3$)), but retro Pf-STN soma stimulation did not (two-way repeated measures ANOVA $F(1,2) = 1.23$, $p = 0.38$, $n = 3$

(**C**) Both terminal Pf-STN (two-way repeated measures ANOVA ($F(1,7) = 62.24$, $p < .0001$, $n = 8$)) and retro Pf-STN soma stimulation (two-way repeated measures ANOVA ($F(1,6) = 27.80$, $p < .0019$, $n = 7$)) significantly increased angular velocity. (**D**) Both terminal Pf-STN (two-way repeated measures ANOVA ($F(1,7) = 33.51$, $p = 0.00071$, $n = 8$)) and retro Pf-STN soma stimulation (two-way repeated measures ANOVA ($F(1,6) = 9.58$, $p = 0.021$, $n = 7$)) caused a significant change in body turning. (**E**) Neither terminal Pf-STN (two-way repeated measures ANOVA ($F(1,7) = 0\ .0018$, $p = 0.97$, $n = 8$)) nor retro Pf-STN soma stimulation (two-way repeated measures ANOVA ($F(1,6) = 0.078$, $p = 0.79$, $n = 7$)) caused a significant lowering of the head. (**F**) Terminal Pf-STN (two-way repeated measures ANOVA ($F(1,7) = 31.89$, $p = 0.00071$, $n = 8$)) but not retro Pf-STN soma stimulation (two-way repeated measures ANOVA ($F(1,6) = 3.35$, $p = 0.021$, $n = 7$)) caused a significant increase in forward velocity. **(G)** Chronos: Stim Epoch: $F(2,12) = 3.59$, $p = 0.06$, $n = 7$. Vglut2: Stim Epoch $F(2,10) = 16.69$, $p = 0.0007$, $n = 6$.

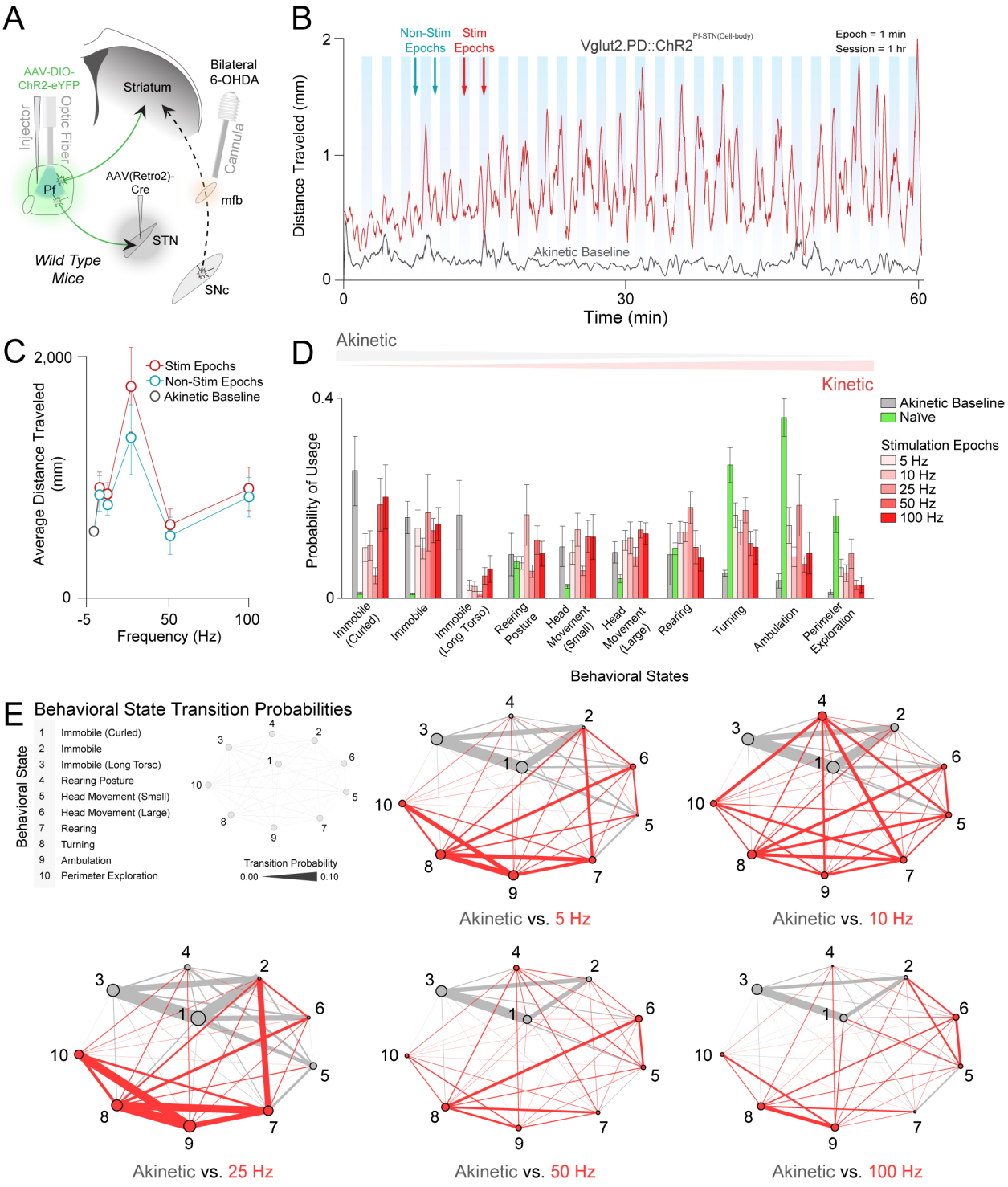

Supplementary Figure 5. Bilateral stimulation of Pf cell bodies that project to the STN rescues akinesia in bilateral-PD mice. (**A**) Generation of bilateral-PD mouse model by injection 6-OHDA through chronically implanted guide cannulae. An injection of rAAV5.EF1α.DIO.hChR2 (H134R).eYFP was made into the Pf after injecting AAV(retro2).hSyn.EF1α.Cre.WPRE into the STN to selectively stimulate Pf cell bodies that project to the STN. (**B**) Representative movement traces are shown for non-stimulation and stimulation epochs for a 25 Hz stimulation session. (**C**) Average distance traveled across stimulation, non-stimulation, and baseline akinetic conditions. (**D**) Probability of usage of AR-HMM identified behavioral states during stimulation epochs across frequencies compared to baseline (Hotellings t-tests, $p < 0.0001$ for all comparisons except 5 Hz ($p > 0.05$)). (**E**) Bigram illustrating transition probabilities of AR-HMM defined behaviors across frequencies versus akinetic baseline.

Supplementary Movies:

Movie S1. Pf unilateral optogenetic excitation

Movie S2. Pf unilateral muscimol inactivation

Movie S3. Pf-STN unilateral terminal excitation

Movie S4. Pf-STN Terminal excitation in bilateral-PD

Movie S5. Pf-STN soma excitation in bilateral-PD

Movie S6. Pf-STN soma inhibition in bilateral-PD

Movie S7. Hidden Markov Behavioral Classification for bilateral-PD

References

1. **C. R. Gerfen, C. J. Wilson, in *Handbook of chemical neuroanatomy,* L. W. Swanson, A. Bjorklund, T. Hokfelt Eds. (Elsevier, Amsterdam, 1996), vol. 12, pp. 371-468.**
2. **J. B. Ding, J. N. Guzman, J. D. Peterson, J. A. Goldberg, D. J. Surmeier, *Neuron* 67, 294 (Jul 29, 2010).**
3. **P. R. Parker, A. L. Lalive, A. C. Kreitzer, *Neuron* 89, 734 (Feb 17, 2016).**
4. **N. Matsumoto, T. Minamimoto, A. M. Graybiel, M. Kimura, *Journal of Neurophysiology* 85, 960 (2001).**
5. **H. D. Brown, P. M. Baker, M. E. Ragozzino, *J Neurosci* 30, 14390 (Oct 27, 2010).**
6. **Y. Smith *et al.*, *Front Syst Neurosci* 8, 5 (2014).**
7. **J. S. Wiegert, M. Mahn, M. Prigge, Y. Printz, O. Yizhar, *Neuron* 95, 504 (Aug 2, 2017).**

8. D. Fan *et al.*, *PLoS One* 6, e22033 (2011).
9. R. A. Bartholomew *et al.*, *Eur J Neurosci* 43, 1097 (Apr, 2016).
10. K. D. Alloway, J. B. Smith, G. D. Watson, *J Neurophysiol* 111, 36 (Jan, 2014).
11. T. Kita, N. Shigematsu, H. Kita, *Eur J Neurosci* 44, 2899 (Dec, 2016).
12. J. Feger, M. Bevan, A. R. Crossman, *Neuroscience* 60, 125 (May, 1994).
13. D. G. Tervo *et al.*, *Neuron* 92, 372 (Oct 19, 2016).
14. A. V. Kravitz *et al.*, *Nature* 466, 622 (Jul 29, 2010).
15. B. Zingg *et al.*, *Neuron* 93, 33 (Jan 4, 2017).
16. G. Di Chiara, M. L. Porceddu, M. Morelli, M. L. Mulas, G. L. Gessa, *Naunyn Schmiedebergs Arch Pharmacol* 306, 153 (Mar, 1979).
17. A. B. Wiltschko *et al.*, *Neuron* 88, 1121 (Dec 16, 2015).
18. V. Gradinaru, M. Mogri, K. R. Thompson, J. M. Henderson, K. Deisseroth, *Science* 324, 354 (Apr 17, 2009).
19. K. J. Mastro *et al.*, *Nat Neurosci* 20, 815 (Jun, 2017).
20. K. J. Mastro, R. S. Bouchard, H. A. Holt, A. H. Gittis, *The Journal of Neuroscience* 34, 2087 (2014).
21. J. Nonnekes *et al.*, *Mov Disord* 31, 1602 (Nov, 2016).
22. J. D. Schaafsma *et al.*, *European journal of neurology* 10, 391 (Jul, 2003).
23. S. Miocinovic, S. Somayajula, S. Chitnis, J. L. Vitek, *JAMA neurology* 70, 163 (Feb, 2013).
24. M. S. Remple *et al.*, *Mov Disord* 26, 1657 (Aug 1, 2011).
25. L. A. Bradfield, J. Bertran-Gonzalez, B. Chieng, B. W. Balleine, *Neuron*, (2013).
26. A. Nambu, H. Tokuno, M. Takada, *Neurosci Res* 43, 111 (Jun, 2002).
27. G. Lopes *et al.*, *Frontiers in neuroinformatics* 9, 7 (2015).
28. G. J. Berman, D. M. Choi, W. Bialek, J. W. Shaevitz, *Journal of the Royal Society, Interface* 11, (Oct 6, 2014).
29. G. Paxinos, K. Franklin, *The mouse brain in stereotaxic coordinates*. (Academic Press, New York, 2003).